Circadian regulation of glutamate release pathways shapes synaptic throughput in the brainstem nucleus of the solitary tract (NTS).

Forrest J. Ragozzino[1], BreeAnne Peterson[1], Ilia N. Karatsoreos[2], and James H. Peters[1*]

*Corresponding author.

1 - Department of Integrative Physiology and Neuroscience
College of Veterinary Medicine
Washington State University
Pullman, WA, USA.

2 - Department of Psychological and Brain Sciences
University of Massachusetts Amherst
Amherst, MA, 01003, USA

Running title: Circadian regulation of brainstem synaptic transmission.

Key words:

Pages: 46
Figures: 8
Tables: 0

Word Count:
Abstract - 193
Introduction - 544
Discussion - 1,678
Total - 9,000

Correspondence:

James H. Peters

Dept. of Integrative Physiology and Neuroscience
Washington State University
1815 Ferdinand's Lane
Pullman, WA, 99164

Phone: 509-335-0157
Fax: 509-335-4650
Email: james_peters@wsu.edu

ACKNOWLEDGMENTS:

This work was supported by grants from the National Institutes of Health (DK092651 to JHP) and (DK119811 to INK), and the National Science Foundation (CAREER 1553067 to INK).

ABSTRACT

Circadian regulation of autonomic reflex pathways pairs physiological function with the daily light cycle. The brainstem nucleus of the solitary tract (NTS) is a key candidate for rhythmic control of the autonomic nervous system. Here we investigated circadian regulation of NTS neurotransmission and synaptic throughput using patch-clamp electrophysiology in brainstem slices from mice. We found that spontaneous quantal glutamate release on to NTS neurons showed strong circadian rhythmicity, with the highest rate of release during the light phase and the lowest in the dark, that were sufficient to drive day / night differences in constitutive postsynaptic action potential firing. In contrast, afferent-evoked action potential throughput was enhanced during the dark and diminished in the light. Afferent-driven synchronous release pathways showed a similar decrease in release probability that did not explain the enhanced synaptic throughput during the night. However, analysis of postsynaptic membrane properties revealed diurnal changes in conductance; which, when coupled with the circadian changes in glutamate release pathways, tuned synaptic throughput between the light and dark phases. These coordinated pre- / postsynaptic changes encode nuanced control over synaptic performance and pair NTS action potential firing and vagal throughput with time of day.

KEYWORDS

vagus, autonomic, clock genes, synaptic throughput

INTRODUCTION

Nearly all physiological processes and behaviors are synchronized to the environmental light cycle (Challet, 2019). The suprachiasmatic nucleus (SCN) of the hypothalamus is the master circadian clock in mammals as it receives direct sensory input from the retina, integrating daily changes in ambient light with anticipatory behavioral and physiological changes of the organism (Hastings et al., 2018). SCN rhythmicity is coupled through a cell-autonomous transcription-translation feedback loop (TTFL) consisting of the rhythmic activity of BMAL and CLOCK transcription factors on E-box promotor regions (Takahashi, 2017). The output of this molecular clock controls circadian rhythmicity in many aspects of physiology; including calcium signaling, membrane potential, synaptic transmission, and endocrine signaling (Harvey et al., 2020). SCN generation of these signals is essential for the circadian control of physiological responses, autonomic reflexes, and associated behaviors. Autonomic tone and feeding behavior are strongly under circadian control, and disruption or desynchronization of these physiological rhythms contributing to many disease states including the progressive development of cardiovascular and metabolic dysregulation, as well as the development of obesity (Karatsoreos et al., 2011). While many studies have focused on understanding rhythm generation in the SCN, much less is known about extra-SCN clock mechanisms. The nucleus of the solitary tract (NTS) in the brainstem is a key candidate for the extra-SCN rhythmic control of autonomic regulation, food intake, processes of satiety, and metabolic regulation (Ritter et al., 2017).

The NTS monitors changes in physiological states and coordinates autonomic regulation of bodily homeostasis (Andresen et al., 1994). Information regarding visceral organ status is relayed to the brain via primary vagal afferent neurons which form strong

93 excitatory contacts onto second-order NTS neurons. In addition to neural input, NTS
94 neurons are also responsive to changes in metabolic status and circulating hormones
95 (Appleyard et al., 2005; Baptista et al., 2005; Cui et al., 2012). Outputs of the NTS control
96 many autonomic reflex pathways as well as feeding, satiety and resulting gastrointestinal
97 physiological responses, all of which possess robust circadian oscillations (Buijs et al.,
98 2006; Konturek et al., 2011; Panda, 2016). Previous studies have demonstrated
99 rhythmicity of clock gene expression in the NTS and the cell bodies of vagal afferent
100 neurons (Herichova et al., 2007; Kaneko et al., 2009; Chrobok et al., 2020), suggesting
101 local TTFL clock signaling. However, the cellular mechanisms through which circadian
102 rhythms orchestrate information processing in the NTS remain unclear. We posit
103 circadian nuanced control of synaptic transmission and action potential throughput
104 mediate these daily changes.

105 Vagal afferent neurons release glutamate via both action potential driven
106 (synchronous and asynchronous) and action potential independent (spontaneous) vesicle
107 release pathways (Wu et al., 2014; Kaeser et al., 2014). While synchronous and
108 asynchronous vesicle release convey real-time action-potential driven signals arising
109 from the viscera, ongoing spontaneous glutamate release sets the synaptic tone and
110 sensitivity to these incoming signals (Shoudai et al., 2010; Kavalali, 2015). It has been
111 well characterized that hormonal and other receptor mediated signals commonly couple
112 to the vesicle release machinery to exert their effects on neural circuits (Appleyard et al.,
113 2005; Bailey et al., 2006; Peters et al., 2008). In this set of studies, we systematically
114 investigate the ability of time of day and circadian regulatory processes to alter pre- and

115 postsynaptic processes to shape constitutive and afferent driven action potential

116 throughput in the NTS.

117

118

RESULTS

The NTS and nodose ganglia have strongly rhythmic TTFL Clock gene expression (Figure 1). Tissue was collected from the NTS and both nodose ganglia at six time points across the day (N = 4 - 5 mice / time point, 25 mice total) from animals under 12:12 LD conditions; and samples were processed using RT-qPCR for quantification of TTFL Clock gene expression levels (**Figure 1A**). Expression for *Per1*, *Per2*, and *NR1D1* (Rev-erbα) showed significant diurnal change in both the NTS and nodose ganglia (**Figure 1B-D**). Whereas *Clock* expression did not significantly change throughout the day (**Figure 1E**), and *Bmal1* (*Arntl1)* was only found to be rhythmic in the nodose tissue (**Figure 1F**).

Rhythmicity of spontaneous glutamate release onto NTS neurons is under circadian control (Figure 2). To investigate the circadian regulation of NTS synaptic transmission we first assayed spontaneous glutamate release parameters across the time-of-day using whole-cell voltage-clamp recordings made from NTS neurons in acute *ex vivo* horizontal brainstem slices (**Figure 2A**). We observed marked differences in the frequency of glutamate mediated spontaneous excitatory postsynaptic currents (sEPSCs) between recordings taken during the light-phase (day) compared to the dark-phase (night) (**Figure 2B**). The average frequency of sEPSCs demonstrated diurnal rhythmicity that peaked during late day (ZT6-12) and was at a minimum during late dark phase (ZT18-24; N = 168 neurons / 14 mice across all times points; **Figure 2C, left panel**). Comparison of sEPSCs frequencies in 12 hr bins showed significantly higher rates of release during the day (7.8 ± 0.9 Hz, N = 72 neurons) compared to the night (3.7 ± 0.3 Hz, N = 92 neurons) (**Figure 2C, right panel**). To determine whether this rhythm was under circadian

control we replicated this experiment from mice placed in constant dark (DD) conditions for 24-42 hours (one full circadian cycle) prior to time of recording. Consistent with clock control, sEPSC frequency remained higher during the relative day (CT 0-12: 5.5 ± 0.5 Hz, N = 61 neurons) compared to relative night (CT 12-24: 4.0 ± 0.4 Hz, N = 55 neurons) with a similar periodicity (Total N = 116 neurons / 15 mice across all times points) (**Figure 2D**). Waveform analysis revealed sEPSC amplitudes were not statistically different across time of day in either the LD (Day: 29.7 ± 1.4 pA, Night: 30.2 ± 1.4 pA) or DD conditions (Day: 27.4 ± 1.5 pA; Night: 32.0 ± 2.1 pA) (**Figure 2E-F**).

To determine whether circadian rhythmicity of sEPSC frequency is secondary to changes in neuronal action potential firing, we replicated our observations in the presence of the voltage activated sodium channel inhibitor tetrodotoxin (TTX, 1μM) (**Figure 3**). Inhibition of action potential firing produced a modest, but statistically significant, decrease in the frequency of spontaneous glutamate release during both the daytime (ZT 4-9) and nighttime (ZT 16-21) recordings (Total N = 29 neurons / 6 mice) (**Figure 3A-B**). However, TTX exposure did not eliminate the day / night difference in sEPSC frequency (**Figure 3B**). The amplitude of sEPSCs was not changed by TTX, consistent with the quantal nature of spontaneous events in the NTS (**Figure 3C**).

Diurnal variations in NTS action potential firing are driven by glutamate signaling. To determine if the changes in glutamate release were sufficient to drive postsynaptic action potential firing, we next performed cell-attached extracellular and whole-cell recordings in *ex vivo* brainstem slices taken between ZT 4-5 for daytime recordings and ZT 16-17 for nighttime recordings (**Figure 4**). We found the NTS had a greater percentage

of neurons spontaneously firing action-potentials at higher frequencies during the day compared to the night (**Figure 4A**). Bath application of ionotropic glutamate receptor antagonists NBQX (25 μM) and D-AP5 (25 μM) eliminated the day / night difference in action potential frequency (**Figure 4A-B**). Further, glutamate receptor antagonism also decreased the proportion of spontaneously firing neurons from 92% to 50% during the day (N = 93 neurons / 6 mice total, Chi-square, ***P < 0.001) and 62% to 33% during the night; eliminating the day / night difference (**Figure 4C**). Whole-cell recordings showed NTS neurons trended toward a more depolarized state and showed higher firing frequencies at rest during the day (**Figure 4D-F**). Together these findings support the role of glutamate to drive rhythmic changes in background NTS neuronal firing; with basal firing greatest during the light and diminished at night.

Day / night differences in the fidelity of throughput at ST-NTS synapses. The fidelity of synaptic throughput reflects the 'attention' of NTS neurons to incoming viscerosensory afferent inputs. Presynaptic activation of ST-afferents produces glutamate dependent action potential firing in NTS neurons (**Figure 5**). The precision of synaptic signaling is the result of both presynaptic release conditions and postsynaptic membrane properties. Similar to previous reports, we found the fidelity of ST-NTS synaptic throughput was high initially, due to elevated initial release probability, but diminished across the stimulus train with a decrease in the precision of action potential initiation and increase in failures becoming more frequent (**Figure 5A**) (Bailey et al., 2006b). Surprisingly, we observed that synaptic throughput was significantly lower in recordings taken during the day compared to the night (**Figure 5B**). To explore this relationship further we repeated the

experiment at both higher and lower stimulus intensities. There was no difference in throughput at lower stimulus intensity (0.1 mA), presumably due to be at or below threshold. Nor was there a significant difference at higher intensities (1 or 3 mA), likely due to recruitment of multiple convergent afferent inputs (**Figure 5C**). Stimulation failed to elicit action potentials in the presence of ionotropic glutamate receptor antagonists NBQX and D-AP5 (*data not shown*).

Immediately following ST synchronized action potentials, many of the NTS neurons showed potentiated firing (44%) with fewer showing transient inhibition (20%) (**Figure 5D, left panel**). Excited neurons had significantly larger post-stimulation action potential burst frequencies during the night compared to neurons recorded in the day (**Figure 5D, middle panel**). While neurons that were inhibited showed no difference in response between time of day (**Figure 5D, right panel**). These data, together with ST synchronized throughput analysis, demonstrate an unexpected greater responsiveness off NTS neurons to afferent driven signals during the night.

Rhythmic changes in solitary tract (ST) evoked synchronous glutamate release. One potential explanation for increased afferent throughput would be for evoked glutamate release to be regulated differently from spontaneous and enhanced during the night while diminished during the day. Spontaneous and evoked vesicle release pathways are known to have many points of opposing control which may explain the differences in spontaneous versus afferent signaling across day and night (Kavalali et al., 2015). We examined primary afferent synaptic transmission by stimulating the ST and recording synchronous EPSC responses onto second order neurons (**Figure 6**). For each neuron

we carefully isolated single afferent inputs using stimulus recruitment protocols; allowing for dissection of release parameters and synaptic performance with minimal contamination from convergent direct and indirect synaptic inputs (Peters et al., 2010; Bailey et al., 2006). Suprathreshold stimulation reliably produced monosynaptic EPSCs which showed no significant difference in EPSC latency to onset (Day: 5.0 ± 0.3 ms vs. Night: 4.8 ± 0.3 ms, T-Test, N = 22 – 23 neurons / 11 mice, P = 0.69) nor synaptic jitter (Day: 105 ± 9 μs vs. Night: 115 ± 9 μs, Mann-Whitney Ranked Sum Test, P = 0.35) between day and night recordings (**Figure 6A**). While evoked EPSC amplitudes varied greatly across neurons (Ranging Day: 72 - 350 pA and Night: 26 – 195 pA) the average initial release (EPSC1) was significantly larger during the day compared to the night (**Figure 6B**). Fluctuation analysis of EPSC1 found an increased covariance (CV) and decreased $1/CV^2$ in recordings during the night consistent with presynaptic changes in either release probability (P_r), number of release site (N), or both (**Figure 6C-D**). Trains of stimuli revealed an increased paired-pulse ratio (PPR) between EPSC1 and 2 during the night but no significant differences in steady-state release (**Figure 6E-F**). These data together suggest that across the day afferent-evoked glutamate release undergoes functional presynaptic changes in initial release parameters with no changes in sustained release mediated by vesicle trafficking.

Following bursts of stimuli, the majority of afferents onto NTS neurons exhibit a distinct asynchronous release profile (Peters et al., 2010). Asynchronous release peaks immediately following the final stimulation and was calculated using the first 100 ms bin. We found asynchronous release was lower during the night but just missed statistical significance (**Figure 6G**). The magnitude of asynchronous release scales with size of the

synchronous EPSC and was likely diminished due to the decrease in evoked release at night, as there was no change in the slope of the asynch / EPSC1 relationship (**Figure 6H**) (Peters et al., 2010)). Thus, because evoked release was suppressed at night, the asynchronous release profile also tended to be smaller; however, there were not obvious day / night differences specific to this release pathway.

Diurnal changes in membrane conductance and intrinsic neuronal excitability. In addition to synaptic inputs, neuronal excitability can be modulated intrinsically via changes to membrane conductances (**Figure 7**). Using voltage-clamp, we first measured current responses to depolarizing voltage steps in neurons recorded during the day and night (**Figure 7A**). There was an increase in the resting membrane current (-100 to -60 mV) during the day compared to night as determined using a current-voltage (I-V) plot (**Figure 7B**). From these data we calculated the slope conductance for each neuron and found it was significantly higher during the day (**Figure 7C**). Using current-clamp, we next assayed the ability of injected current to depolarize the neuron and produce action potential firing (**Figure 7D**). NTS neurons showed a subtle but statistically significant increase in action potential firing frequency during the night (**Figure 7E**). These changes in conductance and excitability suggest that intrinsic membrane properties shape neuronal output in addition to synaptic inputs.

DISCUSSION

The role of circadian rhythms in regulating the timing of physiological processes and behavioral responses is established, and the neurophysiological mechanisms mediating these changes remain of considerable interest. Here, we demonstrate that glutamatergic neurotransmission onto NTS neurons is under circadian regulation with peak release during the light phase. This rhythm coupled with daily changes in NTS membrane conductance drives day/night variation in basal and afferent-evoked neuronal firing. We provide evidence for a temporally coordinated shift from high-level constitutive action potential firing during the light to enhanced vagal afferent-evoked synaptic throughput during the dark (Figure 8). These fundamental circadian shifts in synaptic release pathways and synaptic throughput help explain important differences in autonomic regulation that occurs across the day/night cycle and provides a unique mechanism by which circadian rhythms regulate neuronal circuit performance.

Primary visceral afferent and NTS Clock gene expression.

In this study we observed a clear rhythm of many clock genes in both the nodose ganglia and the NTS. This confirms studies that have previously identified clock rhythmicity in the hindbrain (Kaneko et al., 2009; Herichova et al., 2007; Chrobok et al., 2020) and nodose ganglia (Kentish et al., 2013) and further corroborates the role of the vagal afferent hindbrain circuit as a circadian oscillator. We demonstrate that *Per1*, *Per2*, and *Nr1d1* are in phase between NTS and nodose ganglia neurons. Whereas *Bmal1* was only rhythmic in the nodose ganglia and *Clock* was not rhythmic in either tissue. The molecular clock regulates numerous cellular signaling pathways that are involved in the control of cellular excitability. For example, in the SCN calcium rhythmicity is abated in *Cry1/Cry2* DKO or

Bmal1 KO mice (Noguchi et al., 2017; Enoki et al., 2017). The increasing evidence that this circuit expresses clock rhythmicity indicates a likelihood for similar cellular rhythmicity to the SCN. Previously in the NTS only the rhythmicity in neuronal action potential firing has been explored (Chrobok et al., 2020). Our current findings on synaptic release and synaptic throughput extend and develop our understanding of the circadian coordination of neurophysiology.

Circadian regulated spontaneous glutamate release drives tonic NTS activity.

Here we show that spontaneous glutamate release onto NTS neurons is increased during the light and diminished during the dark, and that this difference persists in constant conditions and in the presence of TTX. Based on previous studies it is possible that this type of rhythm is synapse specific. In the SCN there is conflicting evidence as to whether synaptic release, both glutamate and GABA, is rhythmic (Itri et al., 2004; Lundkvist et al., 2002; Michel et al., 2002). In another case, glutamate release showed diurnal rhythmicity onto lateral habenula (LHb) neurons but not onto hippocampal neurons (Park et al., 2017). One feature that may contribute to the observed rhythm in the present work is the intrinsically high rates of spontaneous release at solitary tract terminals due to the presence of TRPV1 (Shoudai et al., 2010). TRPV1 provides a unique point of control over this synapse because of its high presynaptic expression and role in mediating quantal release (Peters et al., 2010; Shoudai et al., 2010). It has been shown that TRPV1 mRNA expression is under circadian control suggesting circadian changes in the channel could regulate synaptic release (Kimura et al., 2019; Yang et al., 2015)

Another point of control is calcium, however a role for VGCCs in controlling spontaneous release is still under debate. Some studies in the NTS have determined that

spontaneous release is insensitive to VGCC block (Fawley et al., 2016) while others have found VGCCs can regulate spontaneous release (Kline et al., 2019). VGCCs have also been shown to regulate circadian rhythms of firing rates in SCN neurons providing another potential role in regulating neurophysiological rhythms (Enoki et al., 2017b; Pennartz et al., 2002).

Previous studies using organotypic coronal brainstem slices demonstrated a robust circadian rhythm in spontaneous and evoked firing of NTS neurons (Chorbok et al., 2020). The current study demonstrated a rhythm of spontaneous neurotransmission, and that this is sufficient to drive rhythmicity of spontaneous action potential firing of NTS neurons. Spontaneous neurotransmission conveys a large portion of charge transfer in the NTS and selectively increasing or decreasing spontaneous neurotransmission by manipulating temperature modulates action potential firing respectively (Shoudai et al., 2010). This coupling between synaptic transmission and action potential firing has been indicated many times in the SCN. Reducing excitatory postsynaptic activity in the SCN diminishes rhythmicity of SCN firing frequency indicating glutamate may play a role in driving circadian neuronal activity (Lundkvist et al., 2002b). Further, blockade of glutamate receptors reduces both the firing rate and calcium levels of SCN neurons (Michel et al., 2002). This reveals a similarity between the NTS and SCN for a role for glutamate in amplifying circadian firing rates. Another possible role for glutamate is revealed in cultured SCN neurons which only express synchronized circadian firing rhythms once they form synaptic connections (Shirakawa et al., 2000). Whether rhythmic NTS glutamate signaling is a consequence, cause, or both to brainstem circadian rhythmicity remains to be determined.

Afferent evoked release shows rhythmic changes in release probability.

ST-NTS synapses exhibit a high initial release probability (P_r) which is evident by robust frequency dependent depression in response to a train of stimulation (Bailey et al., 2006). Here, we demonstrate diurnal rhythmicity in ST-evoked neurotransmission with peak release occurring during the light. During the dark, we observed a reduced initial evoked EPSC amplitude accompanied by increased EPSC variance and PPR. The coordinated change in both the variance and PPR is indicative of a presynaptic reduction in P_r. P_r can be modulated by many factors and the exact origin of this change is still uncertain. Many proteins that have been shown to regulate presynaptic vesicle fusion, release, and recycling are known to be rhythmic. For example, expression of several voltage gated calcium channels (VGCCs), such as P/Q-type, T-type, and L-type, show circadian rhythmicity in the SCN and cerebellum (Ko et al., 2007; Nahm et al., 2005). In SCN neurons, VGCCs contribute to rhythmic spike generation and intracellular calcium oscillations (Pennartz et al., 2002; Colwell et al., 2000). Other presynaptic proteins, including those that mediate vesicle recycling (Synapsin-I and II), and vesicle fusion (SNAP25, and Munc18), are also rhythmic (Deery et al., 2009; Panda et al., 2002). Alternatively, Pr can be impacted by numerous neuromodulators including corticosterone (Ragozzino et al; 2020), oxytocin (Peters et al., 2008), and vasopressin (Bailey et al., 2006), all of which are under clock control (Kalsbeek et al., 1992; Gillette et al., 1987; Zhang et al., 2011). However, it is unlikely these factors are present at physiological concentrations during *ex vivo* recordings, thus we predict there is likely an *in vivo* role of neuromodulators to amplify or diminish this rhythm. Regardless of the specific

mechanism involved, circadian regulation of presynaptic Pr provides a strong leverage point for controlling circuit activity and constitutive firing.

Intrinsic membrane properties gate neuronal excitability.

One of the more striking observations we made is that peak spontaneous and afferent-evoked action potential firing occur out of phase with each other. This provides an interesting contrast to presynaptic release as it reveals a shift in the preferential mode of signaling between day and night. The neurophysiological control for this difference appears to be changes in the postsynaptic Na^+ leak conductance given our observations of time-of-day changes in the resting membrane conductance of the recorded NTS neurons. Specifically, the membrane conductance is lower during the night producing a 'tighter' membrane more responsive to current injections as a function of Ohm's law. We observed this with the afferent-driven synaptic throughput experiments as well as with directly injecting current and determining the resulting action potential firing frequencies. Previous work has demonstrated that changes in this conductance are is well known to control basal neuronal firing and underly rhythmicity across varying time scales (Impheng et al., 2021; Lu et al., 2007; Simasko et al., 1994). Further, background membrane conductances are proposed to couple and produce an oscillating "bicycle" model where the opposite regulation / expression of resting K+ and Na+ conductances drive rhythmic firing and neural excitability in circadian pacemaker neurons (Flourakis et al., 2015). The extent to which this occurs in NTS neurons is not clear, although we did not measure any obvious changes in K+ conductances. As a consequence of these coordinated presynaptic changes in release probability and postsynaptic changes in membrane conductance, the NTS neurons exhibit this paradoxical increase in intrinsic excitability

and synaptic throughput during the dark phase; whereas during the light basal firing is elevated while afferent synaptic throughput is reduced. These coordinated pre- / postsynaptic changes encode nuanced control over synaptic performance and pair NTS action potential firing and vagal throughput with time of day.

Functional consequences of rhythmic neurophysiological changes.

Many components of the parasympathetic nervous system are under circadian control and previous reports have found that signals that act in the NTS to control metabolic function, including CCK and ghrelin, are rhythmic (Chrobok et al., 2020). CCK effects on food intake also show diurnal variation with peak effectiveness during the inactive phase of the animal (Kraly, 1981). We propose one possible role for rhythmic changes in spontaneous glutamate release and afferent synaptic throughput at this synapse is to provide necessary anticipatory information of rhythmic changes in physiological state including cardiac, respiratory, and digestive rhythms. Increased vagal activity, or parasympathetic tone, is associated with reduced heart rate and respiratory rate, and increased digestive function all of which occur during the inactive phase of the animal (Purnell et al., 2020; Vachon et al., 1987; Hu et al., 2008). This coincides with the observed higher rates of synaptic transmission and basal NTS firing during the light. Furthermore, it is possible that the switch from passive to active signaling enables efficient transmission of viscerosensory signals during the active phase of the animal. Additionally, the NTS projects to the SCN indicating that viscerosensory and interoceptive signals can potentially modulate the clock and that the SCN is likely part of a neural feedback loop which may be involved in regulating autonomic activity (Buijs et al, 2003; Buijs et al., 2014).

MATERIALS AND METHODS

Animals:

Adult male C57BL/6N mice (20 - 30 g) were obtained from either Envigo or Jackson laboratories. Mice were maintained under standard 12:12 hour light – dark (LD) cycle in a temperature-controlled (23 ± 1 °C) room with *ad libitum* access to water and standard pellet chow. For experiments involving constant darkness (12:12 hour dark – dark (DD), animals were house in identical conditions except for constant darkness for 24-42 hours prior to experimentation. All experiments were performed in accordance with procedures approved by the Institutional Animal Use and Care Committee (IACUC) at Washington State University.

Molecular biology:

Tissue preparation: Mice were deeply anesthetized and euthanized at six time points across the circadian cycle: ZT0, ZT4, ZT8, ZT12, ZT 16, and ZT 20 (N = 4 mice / time-point, 24 mice total). Brainstems and nodose ganglia were isolated and flash frozen on dry ice and stored at -80°C. Brainstems, separated rostral to the cerebellum, were mounted on a Leica cryostat and cut on the coronal plane producing 3 x 300 μm thick slices that were direct mounted onto frozen glass slides. From these slices we collected NTS enriched tissue using a 0.5 mm diameter tissue punch. All collected tissues were stored in RNAlater (ThermoFisher).

RT-qPCR: The tissue was processed for RNA extraction using Qiazol extraction and RNeasy Micro Kit (QIAGEN). Concentrations of mRNA were determined using spectrophotometry with samples diluted to the same final concentration. Immediately

following extraction, mRNA was treated with Ambion DNase treatment and removal (Life Technologies) and cDNA synthesis was performed with QuantiTect® cDNA reverse transcription kit (QIAGEN). Reverse-transcription qPCR assays were performed using TaqMan chemistry commercially available validated assays from Life Technologies. Transcripts were amplified on a 7500 Fast Real-Time PCR System by Applied Biosystems (Life Technologies) using TaqMan probes for *Rn18s* (control gene; Mm03928990_g1), *Per1* (Mm00501813_m1), *Per2* (Mm00478099_m1), *Bmal1* (*Arntl1*) (Mm00500226_m1), *Nr1d1* (Rev-erbα) (Mm00520708_m1), *Clock* (Mm00455950_m1), *Cckar* (Mm00438060_m1), *Cckbr* (Mm00432329_m1). Samples were run in triplicate with a standardized 5 ng (2.5 ng / μL x 2 μL) of cDNA and compared using the $^{\Delta\Delta}$CT method of relative quantification, with *Rn18s* used as the control housekeeping gene and ZT0 values as the relative target. Kruskal-Wallis test with post-hoc multiple comparison was performed for statistical analysis.

Slice electrophysiology:

Horizontal brainstem slice preparation: Brainstem slices were isolated from mice deeply anesthetized with isoflurane as previously described (Appleyard et al., 2005). The brainstem was removed from just rostral to the cerebellum to the first cervical vertebrae and placed in ice-cold artificial cerebral spinal fluid (aCSF) containing (mM): 125 NaCl, 3 KCl, 1.2 KH_2PO_4, 1.2 $MgSO_4$, 25 $NaHCO_3$, 2 $CaCl_2$, and 10 dextrose, bubbled with 95% O_2 – 5% CO_2. aCSF was brought to a pH of 7.40 using 1M HCl. Once chilled, the tissue was cut to remove the cerebellum and the tissue block was mounted horizontally to a pedestal with cyanoacrylate glue and submerged in cold aCSF on a vibrating microtome

(Leica VT1200S). Approximately 150-200 µm was removed from the dorsal surface and then a single 250 µm thick horizontal slice was collected containing the solitary tract (ST) along with the neuronal cell bodies of the medial NTS region. Slices were cut with a sapphire knife (Delaware Diamond Knives, Wilmington, DE) and secured using a fine polyethylene mesh in a perfusion chamber with continuous perfusion of aCSF bubbled with 95% O_2 – 5% CO_2 at 32 °C. Brainstem slices were generated at 6-hour intervals, starting at zeitgeber time (ZT) 0, and data were binned with reference to the time of each recording; either every 4 hours or into day (ZT0-12) and night (ZT12-24). In some experiments where only two time points were used, slices were taken between ZT4-5 and ZT16-17.

Whole cell patch-clamp recordings: Recordings were performed on NTS neurons contained in horizontal brainstem slices using an upright Nikon FN1 microscope with a Nikon DS-Qi1Mc digital camera and NIS-elements AR imaging software. Recording electrodes (3.0 – 4.5 MΩ) were filled with one of two intracellular solutions containing either (Cs-internal, mM): 10 CsCl, 130 Cs-Methanesulfonate, 11 EGTA, 1 $CaCl_2$, 2 $MgCl_2$, 10 HEPES, 2 Na_2ATP, and 0.2 Na_2GTP; or (K+ internal, mM) 6 NaCl, 4 NaOH, 130 K-gluconate, 11 EGTA, 1 $CaCl_2$, 1 $MgCl_2$, 10 HEPES, 2 Na_2ATP, and 0.2 Na_2GTP. For measurements of excitatory post-synaptic currents (EPSCs), neurons were studied under voltage-clamp conditions with an MultiClamp 700A amplifier (Molecular Devices, Union City, CA) and held at V_H = -60 mV in whole-cell patch configuration. Only recordings with a series resistance of <20 MΩ were used for experiments to ensure good access and

maintenance of voltage-clamp. Signals were filtered with a 1 kHz bezel filter and sampled at 20 kHz using Axon pClamp10 software (Molecular Devices).

Extracellular recordings: To monitor action potential firing in single NTS neurons with unperturbed intracellular conditions we utilized loose-seal extracellular recordings. Recording pipets (3.0 – 4.5 MΩ) were filled with the standard extracellular aCSF and a relatively low resistance (loose) seal was formed with the NTS neuron. The typical seal resistance was between 10 - 20 MΩ and neurons were recorded in the current-clamp configuration with no injected current. This allowed for stable recordings and the clear resolution of single-unit extracellular spikes resulting from spontaneous and evoked action potential firing.

Solitary tract stimulation: Second-order neurons in the NTS receive direct innervation from ST afferents, which include the primary vagal afferent terminals, and can be identified based on the precision of shock evoked synchronous glutamate release. To selectively activate ST afferent fibers, a concentric bipolar stimulating electrode (200 µm outer tip diameter; Frederick Haer Co., Bowdoinham, ME, USA) was placed on distal portions of the visible ST rostral to the recording region. We delivered a train of five current shocks to the ST (60 µs shock duration at 25 Hz, 6 s inter-stimulus interval) using a Master-8 isolated stimulator (A.M.P.I., Jerusalem, Israel). Input latency, the time between the shock artifact and onset of the synchronous EPSC, and synaptic “jitter”, the standard deviation of the latency, were measured to identify monosynaptic inputs. Jitters of <200

484 µs identify monosynaptic afferent inputs onto the NTS neuron (Doyle and Andresen,
485 2001).

486

487 *Data analysis:* For brainstem slice recordings the digitized waveforms of action potentials
488 and synaptic events were analyzed using an event detection and analysis program
489 (MiniAnalysis, Synaptosoft, Decatur, GA). Analysis for all ST-stimulated currents was
490 accomplished using Clampfit 10 (Molecular Devices). For quantal, spontaneous
491 glutamate release, all events >10 pA were counted for frequency values. Fitting of quantal
492 EPSC amplitudes and decay kinetics (90-10%) was performed using a fitting protocol
493 (MiniAnalysis) on > 500 discrete events or 5 minutes of recording time if less than 500
494 events occurred.

495

496 *Chemicals and drugs:* Drugs were purchased from retail distributers including tetrodotoxin
497 (TTX, 1 µM; Tocris #1069), 2,3-dioxo-6-nitro-7-sulfamoyl-benzoquinoxaline (NBQX, 25
498 µM; Tocris #0373), D-2-Amino-5-phosphonopentanoic acid (D-AP5, 25 µM; Tocris
499 #0106). These were stored as stock aliquots and diluted in fresh aCSF to their final
500 concentration the day of recording. The general salts used for making bath solutions were
501 purchased from Sigma-Aldrich. All drugs were delivered via bath perfusion at a flow rate
502 of ~2 mL / min and slices were allowed to fully recover before the start of recording.

503

504 **Statistical analyses:**

505 For statistical comparisons we used Sigma Stat software (Systat Software Inc., San Jose,
506 CA). The data were tested for normality and equal variance and the appropriate

parametric or nonparametric statistics were used; including, ANOVA with post hoc analysis, T-tests, Mann Whitney Rank Sum test, and linear regression analysis. Data sets were analyzed using Grubb's test and extreme outlier values were excluded from statistical comparisons. Specific test used are indicated in the results section. Comparisons were considered statistically different with an alpha level of $P < 0.05$.

512 *ACKNOWLEDGMENTS*

513 Author contributions.

514 Design experiments (*FJR, INK, JHP*).

515 Conduct experiments (*FJR, BP, JHP*).

516 Analyze data (*FJR, BP, INK, JHP*).

517 Prepare and write manuscript (*FJR, INK, JHP*).

518

519 REFERENCES

520 Andresen, M. C. & Kunze, D. L. Nucleus Tractus Solitarius—Gateway to Neural
521 Circulatory Control. *Annual Review of Physiology* 56, 93–116 (1994).

522 Appleyard, S. M. *et al.* Proopiomelanocortin Neurons in Nucleus Tractus Solitarius Are
523 Activated by Visceral Afferents: Regulation by Cholecystokinin and Opioids. *J. Neurosci.*
524 25, 3578–3585 (2005).

525 Bailey, T. W., Jin, Y.-H., Doyle, M. W., Smith, S. M. & Andresen, M. C. Vasopressin
526 Inhibits Glutamate Release via Two Distinct Modes in the Brainstem. *Journal of*
527 *Neuroscience* 26, 6131–6142 (2006).

528 Bailey, T. W., Hermes, S. M., Andresen, M. C., Aicher, S. A. Cranial visceral afferent
529 pathways through the nucleus of the solitary tract to caudal ventrolateral medulla or
530 paraventricular hypothalamus: target-specific synaptic reliability and convergence
531 patterns. *J Neurosci*. 15, 11893-11902 (2006b).

532 Baptista, V., Zheng, Z. L., Coleman, F. H., Rogers, R. C. & Travagli, R. A. Cholecystokinin
533 Octapeptide Increases Spontaneous Glutamatergic Synaptic Transmission to Neurons of
534 the Nucleus Tractus Solitarius Centralis. *Journal of Neurophysiology* 94, 2763–2771
535 (2005).

536 Buijs, R. M. *et al.* The suprachiasmatic nucleus balances sympathetic and
537 parasympathetic output to peripheral organs through separate preautonomic neurons.
538 *Journal of Comparative Neurology* 464, 36–48 (2003).

539 Buijs RM, Scheer FA, Kreier F, Yi C, Bos N, Goncharuk VD, Kalsbeek A. 2006.
540 Organization of circadian functions: interaction with the body. Prog Brain Res 153:341–
541 360. doi:10.1016/S0079-6123(06)53020-1

542 Buijs, F. N. *et al.* The suprachiasmatic nucleus is part of a neural feedback circuit adapting
543 blood pressure response. *Neuroscience* 266, 197–207 (2014).

544 Challet, E. The circadian regulation of food intake. *Nature Reviews Endocrinology* 15,
545 393–405 (2019).

546 Chrobok, L. *et al.* Timekeeping in the hindbrain: a multi-oscillatory circadian centre in the
547 mouse dorsal vagal complex. *Communications Biology* 3, 1–12 (2020).

548 Colwell, C. S. Circadian modulation of calcium levels in cells in the suprachiasmatic
549 nucleus. *Eur J Neurosci* 12, 571–576 (2000).

550 Cui, R. J., Roberts, B. L., Zhao, H., Zhu, M. & Appleyard, S. M. Serotonin activates
551 catecholamine neurons in the solitary tract nucleus by increasing spontaneous glutamate
552 inputs. *J Neurosci* 32, 16530–16538 (2012).

553 Deery, M. J. *et al.* Proteomic Analysis Reveals the Role of Synaptic Vesicle Cycling in
554 Sustaining the Suprachiasmatic Circadian Clock. *Current Biology* 19, 2031–2036 (2009).

555 Doyle, M. W., Andresen, M. C. Reliability of monosynaptic sensory transmission in brain
556 stem neurons in vitro. *J Neurophysiol* 85(5):2213-23 (2001).

557 Enoki, R., Ono, D., Kuroda, S., Honma, S. & Honma, K. Dual origins of the intracellular
558 circadian calcium rhythm in the suprachiasmatic nucleus. *Scientific Reports* 7, 41733
559 (2017).

560 Enoki, R. *et al.* Synchronous circadian voltage rhythms with asynchronous calcium
561 rhythms in the suprachiasmatic nucleus. *Proc. Natl. Acad. Sci. U.S.A.* 114, E2476–E2485
562 (2017b).

563 Fawley, J. A., Hofmann, M. E. & Andresen, M. C. Distinct Calcium Sources Support
564 Multiple Modes of Synaptic Release from Cranial Sensory Afferents. *J. Neurosci.* 36,
565 8957–8966 (2016).

566 Flourakis, M. *et al.* A Conserved Bicycle Model for Circadian Clock Control of Membrane
567 Excitability. *Cell* 162, 836–848 (2015).

568 Gillette, M. U. & Reppert, S. M. The hypothalamic suprachiasmatic nuclei: Circadian
569 patterns of vasopressin secretion and neuronal activity in vitro. *Brain Research Bulletin*
570 19, 135–139 (1987).

571 Harvey, J. R. M., Plante, A. E. & Meredith, A. L. Ion Channels Controlling Circadian
572 Rhythms in Suprachiasmatic Nucleus Excitability. *Physiological Reviews* 100, 1415–1454
573 (2020).

574 Hastings, M. H., Maywood, E. S. & Brancaccio, M. Generation of circadian rhythms in the
575 suprachiasmatic nucleus. *Nature Reviews Neuroscience* 19, 453–469 (2018).

576 Herichová, I. *et al.* Rhythmic clock gene expression in heart, kidney and some brain nuclei
577 involved in blood pressure control in hypertensive TGR(mREN-2)27 rats. *Mol Cell*
578 *Biochem* 296, 25–34 (2007).

579 Hu, K., Scheer, F. A. J. L., Buijs, R. M. & Shea, S. A. The circadian pacemaker generates
580 similar circadian rhythms in the fractal structure of heart rate in humans and rats.
581 *Cardiovascular Research* 80, 62–68 (2008).

582 Impheng, H. *et al.* The sodium leak channel NALCN regulates cell excitability of pituitary
583 endocrine cells. *The FASEB Journal* 35, e21400 (2021).

584 Itri, J., Michel, S., Waschek, J. A. & Colwell, C. S. Circadian Rhythm in Inhibitory Synaptic
585 Transmission in the Mouse Suprachiasmatic Nucleus. *Journal of Neurophysiology* 92,
586 311–319 (2004).

587 Kaeser, P. S. & Regehr, W. G. Molecular Mechanisms for Synchronous, Asynchronous,
588 and Spontaneous Neurotransmitter Release. *Annu Rev Physiol* 76, 333–363 (2014).

589 Kalsbeek, A., Buijs, R. M., van Heerikhuize, J. J., Arts, M. & van der Woude, T. P.
590 Vasopressin-containing neurons of the suprachiasmatic nuclei inhibit corticosterone
591 release. *Brain Research* 580, 62–67 (1992).

592 Kaneko, K. *et al.* Obesity alters circadian expressions of molecular clock genes in the
593 brainstem. *Brain Research* 1263, 58–68 (2009).

594 Karatsoreos, I. N., Bhagat, S., Bloss, E. B., Morrison, J. H. & McEwen, B. S. Disruption
595 of circadian clocks has ramifications for metabolism, brain, and behavior. *Proc Natl Acad*
596 *Sci U S A* 108, 1657–1662 (2011).

597 Kavalali, E. T. The mechanisms and functions of spontaneous neurotransmitter release.
598 *Nat. Rev. Neurosci.* 16, 5–16 (2015).

599 Kentish, S. J., Frisby, C. L., Kennaway, D. J., Wittert, G. A. & Page, A. J. Circadian
600 variation in gastric vagal afferent mechanosensitivity. *J. Neurosci.* 33, 19238–19242
601 (2013).

602 Kimura, Y. *et al.* The circadian rhythm of bladder clock genes in the spontaneously
603 hypersensitive rat. *PLOS ONE* 14, e0220381 (2019).

604 Kline, D. D., Wang, S. & Kunze, D. L. TRPV1 channels contribute to spontaneous
605 glutamate release in nucleus tractus solitarii following chronic intermittent hypoxia.
606 *Journal of Neurophysiology* 121, 881–892 (2019).

607 Ko, M. L., Liu, Y., Dryer, S. E. & Ko, G. Y.-P. The expression of L-type voltage-gated
608 calcium channels in retinal photoreceptors is under circadian control. *J Neurochem* 103,
609 784–792 (2007)

610 Konturek PC, Brzozowski T, Konturek SJ. 2011. Gut clock: implication of circadian
611 rhythms in the gastrointestinal tract. J Physiol Pharmacol 62:139–150.

612 Kraly, F. S. A diurnal variation in the satiating potency of cholecystokinin in the rat.
613 *Appetite* 2, 177–191 (1981).

614 Lu, B. *et al.* The Neuronal Channel NALCN Contributes Resting Sodium Permeability and
615 Is Required for Normal Respiratory Rhythm. *Cell* 129, 371–383 (2007).

616 Lundkvist, G. B., Kristensson, K. & Hill, R. H. The Suprachiasmatic Nucleus Exhibits
617 Diurnal Variations in Spontaneous Excitatory Postsynaptic Activity. *Journal of Biological*
618 *Rhythms* 17, 40–51 (2002).

619 Lundkvist, G. B., Hill, R. H. & Kristensson, K. Disruption of Circadian Rhythms in Synaptic
620 Activity of the Suprachiasmatic Nuclei by African Trypanosomes and Cytokines.
621 *Neurobiology of Disease* 11, 20–27 (2002b).

622 Michel, S., Itri, J. & Colwell, C. S. Excitatory Mechanisms in the Suprachiasmatic Nucleus:
623 The Role of AMPA/KA Glutamate Receptors. *J Neurophysiol* 88, 817–828 (2002).

624 Nahm, S.-S., Farnell, Y. Z., Griffith, W. & Earnest, D. J. Circadian Regulation and Function
625 of Voltage-Dependent Calcium Channels in the Suprachiasmatic Nucleus. *J. Neurosci.*
626 25, 9304–9308 (2005).

627 Noguchi, T. *et al.* Calcium Circadian Rhythmicity in the Suprachiasmatic Nucleus: Cell
628 Autonomy and Network Modulation. *eNeuro* 4, ENEURO.0160-17.2017 (2017).

629 Panda, S. *et al.* Coordinated Transcription of Key Pathways in the Mouse by the Circadian
630 Clock. *Cell* 109, 307–320 (2002).

631 Buijs RM, Scheer FA, Kreier F, Yi C, Bos N, Goncharuk VD, Kalsbeek A. 2006.
632 Organization of circadian functions: interaction with the body. Prog Brain Res 153:341–
633 360. doi:10.1016/S0079-6123(06)53020-1

634 Konturek PC, Brzozowski T, Konturek SJ. 2011. Gut clock: implication of circadian
635 rhythms in the gastrointestinal tract. J Physiol Pharmacol 62:139–150.

636 Panda S. 2016. Circadian physiology of metabolism. Science 354:1008–1015.
637 doi:10.1126/science.aah4967

638 Park, H., Cheon, M., Kim, S. & Chung, C. Temporal variations in presynaptic release
639 probability in the lateral habenula. *Scientific Reports* 7, 40866 (2017).

640 Pennartz, C. M. A., Jeu, M. T. G. de, Bos, N. P. A., Schaap, J. & Geurtsen, A. M. S.
641 Diurnal modulation of pacemaker potentials and calcium current in the mammalian
642 circadian clock. *Nature* 416, 286 (2002).

643 Peters, J. H. *et al.* Oxytocin Enhances Cranial Visceral Afferent Synaptic Transmission to
644 the Solitary Tract Nucleus. *Journal of Neuroscience* 28, 11731–11740 (2008).

645 Peters, J. H., McDougall, S. J., Fawley, J. A., Smith, S. M. & Andresen, M. C. Primary
646 afferent activation of thermosensitive TRPV1 triggers asynchronous glutamate release at
647 central neurons. *Neuron* 65, 657–669 (2010).

648 Purnell, B. S. & Buchanan, G. F. Free-running circadian breathing rhythms are eliminated
649 by suprachiasmatic nucleus lesion. *Journal of Applied Physiology* 129, 49–57 (2020).

650 Ragozzino, F. J. *et al.* Corticosterone inhibits vagal afferent glutamate release in the
651 Nucleus of the Solitary Tract via retrograde endocannabinoid signaling. *American Journal*
652 *of Physiology-Cell Physiology* ajpcell.00190.2020 (2020)
653 doi:10.1152/ajpcell.00190.2020.

654 Ritter, R. C., Campos, C. A., Nasse, J. & Peters, J. H. Vagal Afferent Signaling and the
655 Integration of Direct and Indirect Controls of Food Intake. in *Appetite and Food Intake:*
656 *Central Control* (ed. Harris, R. B. S.) (CRC Press/Taylor & Francis, 2017).

657 Shirakawa, T., Honma, S., Katsuno, Y., Oguchi, H. & Honma, K. Synchronization of
658 circadian firing rhythms in cultured rat suprachiasmatic neurons. *European Journal of*
659 *Neuroscience* 12, 2833–2838 (2000).

660 Shoudai, K., Peters, J. H., McDougall, S. J., Fawley, J. A. & Andresen, M. C. Thermally
661 active TRPV1 tonically drives central spontaneous glutamate release. *J Neurosci* 30,
662 14470–14475 (2010).

663 Simasko, S. M. A background sodium conductance is necessary for spontaneous
664 depolarizations in rat pituitary cell line GH3. *American Journal of Physiology-Cell*
665 *Physiology* 266, C709–C719 (1994).
666 Takahashi, J. S. Transcriptional architecture of the mammalian circadian clock. *Nat Rev*
667 *Genet* 18, 164–179 (2017).

668 Vachon, C. & Savoie, L. Circadian variation of food intake and digestive tract contents in
669 the rat. *Physiology & Behavior* 39, 629–632 (1987).

670 Wu, S., Fenwick, A. J. & Peters, J. H. Channeling satiation: a primer on the role of TRP
671 channels in the control of glutamate release from vagal afferent neurons. *Physiol. Behav.*
672 136, 179–184 (2014).

673 Yang, S.-C., Chen, C.-L., Yi, C.-H., Liu, T.-T. & Shieh, K.-R. Changes in Gene Expression
674 Patterns of Circadian-Clock, Transient Receptor Potential Vanilloid-1 and Nerve Growth
675 Factor in Inflamed Human Esophagus. *Sci Rep* 5, 13602 (2015).

676 Zhang, G. & Cai, D. Circadian intervention of obesity development via resting-stage
677 feeding manipulation or oxytocin treatment. *Am J Physiol Endocrinol Metab* 301, E1004–
678 E1012 (2011).
679

680 FIGURE LEGENDS

681 **FIGURE 1: Rhythmic clock gene expression in NTS and vagal afferent neurons**
682 **across time of day. A)** Clock gene expression was determined in the NTS and nodose
683 ganglia using RT-qPCR from tissues taken at six time points throughout the light/dark
684 cycle. For each time point tissue was collected from N = 4 - 5 mice and samples were run
685 in triplicate. Canonical clock gene expression from nodose ganglia (squares) and NTS
686 (circles) show rhythmic changes for **B)** *Per1* (NTS: ANOVA, $^{\#}P = 0.039$; Nodose: ANOVA,
687 ***P < 0.001) , **C)** *Per2* (NTS: ANOVA, $^{\#}P = 0.01$; Nodose: Kruskal-Wallis, **P = 0.003),
688 **D)** *Nr1d1* (Rev-erbα) (NTS: Kruskal-Wallis, $^{\#}P = 0.032$; Nodose: Kruskal-Wallis, ***P <
689 0.001); but not for **E)** *Clock* (NTS: ANOVA, P = 0.44; Nodose: ANOVA, P = 0.48), and **F)**
690 only in nodose tissue, but not NTS, for *Arntl1* (Bmal1) (NTS: ANOVA, P = 0.62; Nodose:
691 Kruskal-Wallis, *P = 0.031). $^{\Delta\Delta}$Ct was calculated relative to RN18s and ZT0, with data
692 expressed as a fold-change on a log base 2 scale.

693

694 **FIGURE 2: Spontaneous glutamate release frequency shows circadian rhythmicity.**
695 **A)** Infrared-DIC images of a mouse horizontal brain slice (top) and whole-cell recording
696 of a single NTS neuron (bottom) during patch-clamp experiments. NTS, nucleus of the
697 solitary tract; ST, solitary tract; 4V, fourth ventricle. Cells were voltage-clamped at -60
698 mV. **B)** Representative current traces showing spontaneous EPSCs (sEPSCs) from
699 recordings in slices taken at one of four time-points throughout the day: ZT 0, ZT 6, ZT
700 12, and ZT 18. **C)** Average sEPSC frequency recorded from animals housed under 12:12
701 LD conditions plotted in four-hour bins across time-of-day showing the change in
702 frequency (left panel). Frequency of release was significantly different during the day (ZT

0-12) when compared to the night (ZT 12-24) (right panel) (N = 72 – 92 neurons / 14 mice, Mann-Whitney Rank Sum Test, **P < 0.001). **D)** Recordings from mice taken after 24-42 hrs of constant darkness (12:12 DD) maintained rhythmicity of sEPSC frequency independent of light cues. Frequency was significantly higher from cells taken during the respective day (CT 0-12) compared to the dark (CT 12-24) (N = 55 – 61 neurons / 15 mice, Mann-Whitney Rank Sum Test, **P = 0.01). **E)** Average sEPSC waveforms across time of day. Traces are averages of 100 discrete events from representative recordings. **F)** There was no significant difference in sEPSC amplitude between day and night in LD (Mann-Whitney Rank Sum Test, P = 0.89) or DD conditions (Mann-Whitney Rank Sum Test, P = 0.14).

FIGURE 3: Rhythmic changes in spontaneous glutamate release occur independent of action potential firing. A) Representative current traces showing spontaneous events before and after bath perfusion of tetrodotoxin (TTX, 1 μM) during daytime and nighttime recordings. **B)** Bath application of TTX reduced the sEPSC frequency during day (Paired T-test, N = 16 neurons / 3 mice, *P = 0.015) and night (Paired T-test, N = 13 neurons / 3 mice, *P = 0.012) but failed to eliminate the day/night difference (Control Day/Night: Mann-Whitney Rank Sum Test, N = 13 – 16 neurons / 6 mice, *P = 0.04; and TTX Day/Night: Mann-Whitney Rank Sum Test, N = 13 – 16 neurons / 6 mice, *P = 0.05). **C)** Exposure to TTX had no effect on sEPSC amplitude during either the day (Paired T-test, P = 0.80) or night (Paired T-Test, P = 0.35).

FIGURE 4: Glutamate drives diurnal rhythmicity in basal action potential firing. A) Representative extracellular voltage traces showing spontaneous action potentials during the day (ZT5-9) and night (ZT17-21) under control conditions and following bath application of ionotropic glutamate antagonists (NBQX 25 μM and AP5 25 μM). **B)** Baseline action potential frequency was significantly greater during the day compared to night (Mann-Whitney Rank Sum Test, N = 50 - 53 neurons / 6 mice, ***P < 0.001). Bath application of NBQX + AP5 lowered frequency during the day (Mann-Whitney Rank Sum Test, N = 44 – 50 neurons / 6 mice, ***P < 0.001) and night (Mann-Whitney Rank Sum Test, N = 46 – 53 neurons / 6 mice, ***P < 0.001); eliminating the day / night difference in action potential firing (Mann-Whitney, N = 44 – 46 neurons / 6 mice, P = 0.12). **C)** Similarly, the percent of neurons firing action potentials spontaneously under control conditions was greater during the day compared to the night (Chi-square, N = 103 neurons / 6 mice, ***P < 0.001). This day / night difference was reduced following NBQX + AP5 and no longer statistically significant (Chi-square, N = 100 neurons / 6 mice, P = 0.21). **D)** Whole-cell recordings from NTS neurons confirmed the day / night difference in action potential frequency. **E)** While there was no significant difference in the resting membrane potentials (RMP) (T-test, N = 32 – 35 neurons / , P = 0.08) spontaneous action potential firing frequencies were significantly faster during the day (**F**, Mann-Whitney Ranked Sum Test, N = 32 – 35 neurons / , *P = 0.03).

FIGURE 5: Paradoxical increase in afferent-evoked synaptic throughput at night. A) Representative traces showing evoked action potentials by 0.5 mA stimulations at 25 Hz from cell-attached recordings of NTS neurons. Insets show individual action potentials

evoked after shock 1 (left), shock 5 (middle), and shock 10 (right). Red traces denote failures. **B)** Plot of the throughput (% successes) of individual stimulations over a train of 10 ST shocks at 0.5 mA stimulation intensity during daytime (ZT5-9) and nighttime (ZT17-21) recordings. At 0.5 mA stim intensity there was a statistical interaction between stimulus number and timed of day with throughput was significantly higher during the night (2-way ANOVA, N = 30 – 39 neurons / 6 mice, ***P < 0.001). **C)** Recruitment curve of action potential throughput at increasing stimulation intensities. There was a significant interaction between time of day and stimulus intensity with throughput was higher at night (2-way ANOVA, N = 30 -39 neurons / 6 mice, **P = 0.008). Post hoc analysis showed a significant difference in throughput at an intermediate stimulus intensity (0.5 mA) (Bonferroni corrected T-Test, N = 30 – 39 neurons / 6 mice, **P = 0.006) but not at very high (1 mA: P = 0.25 and 3 mA: P = 0.72) or low intensities (0.1 mA: P = 0.71). **D)** Representative traces of excited (top) and inhibited (bottom) post-simulation responses. Neurons recorded during the night had a significantly larger post-stimulation excitatory responses compared to day (T-Test, N = 13 – 19 neurons / 6 mice, *P = 0.03). There was no significant difference in the less common inhibitory responses between day or night (T-Test, N = 6 – 7 neurons / 6 mice, P = 0.61).

FIGURE 6: FIGURE 6: Day / night differences in evoked synchronous glutamate release consistent with presynaptic regulation of the probability of release. A) Representative current traces showing 25 Hz suprathreshold stimulation of solitary-tract (ST) afferents and resulting synchronous EPSCs (ST-EPSCs) recorded from slices taken in the day compared to the slices taken at night. Arrows denote time of ST shocks with

traces shown as an overlay of 10 individual trials. **B)** The average ST-EPSC amplitude was significantly smaller in recordings made at night compared to the day (T-Test, N = 23 – 27 neurons / 11 mice, **P = 0.002). **C)** The amplitude variability of EPSC1, Coefficient of variance (CV), was significantly higher in recordings made at night (Mann-Whitney Rank Sum Test, **P = 0.004). **D)** Due to this difference in CV, $1/CV^2$ was significantly higher during the day compared to the night (Mann-Whitney Rank Sum Test, **P = 0.004). **E)** As a result of changes in EPSC1, the paired-pulse ratio (PPR) was significantly higher at night compared to the day (T-Test, N = 23 – 27 neurons / 11 mice, ***P = 0.0004). **F)** Average ST-EPSC amplitude across five shocks show a significant difference between day and night (2-way RM ANOVA, N = 42 neurons / 11 mice, ***P < 0.001). Post hoc analysis confirmed EPSC1, but not EPSC2-5, was significantly smaller during the night compared to recordings made during the day (Bonferroni corrected T-Test, EPSC1: ***P < 0.001, EPSC2: P = 0.29, EPSC3: P = 0.21, EPSC4: P = 0.66, EPSC5: P = 0.83). **G)** Afferent-evoked asynchronous EPSCs, elicited by a series of five ST shocks, were not statistically different between day and night recordings (Mann-Whitney Rank Sum Test, N = 27 – 31 neurons / 11 mice, P = 0.053). **H)** Plot of asynchronous release as a function of EPSC1 amplitude. There was no significant difference in the slope of the EPSC1 to asynchronous frequency relationship between day and night (Mann-Whitney Rank Sum Test, N = 27 – 31 neurons / 11 mice, P = 0.67). Summary data boxplots show the mean (long gray bar) median (short black bar) with 25-75%, and 10-90% whisker length.

FIGURE 7: Rhythmic changes in postsynaptic NTS whole-cell conductances impact action potential firing sensitivity to injected current. A) Voltage-clamp current traces from NTS neurons demonstrating the current-voltage (I-V) relationship in NTS neurons during day and night. Inset shows the step protocol with 10 mV step intervals from -100 mV to -60 mV. **B)** Plot of the average I-V curves from recordings during the day and night. Values are the average ± stdev of steady-state current density. **C)** The average calculated slope conductance of neurons recorded at night was lower than that of neurons recorded during the day (T-test, N = 67 – 92 neurons / 14 mice, *P = 0.017). **D)** Representative voltage traces from NTS neurons held at -60 mV showing action potential firing elicited during a 1 s, 40 pA, current injection during day (top) and night (bottom) recordings. **E)** Summary plot showing the subtle, but statistically significant, differences between day and night in the action potential firing rate in response to increasing current injections (Mann-Whitney Rank Sum Test, N = 32 – 35 neurons / 6 mice, *P = 0.026).

FIGURE 8: Changes in glutamate release and intrinsic membrane properties shift synaptic processing in the NTS. Model diagram summarizing the observed changes in synaptic function across time of day. **A-B)** During the light phase high spontaneous glutamate release drives elevated postsynaptic action potential firing, while increased postsynaptic membrane conductance diminishes afferent driven throughput. Together this produces a high tone / low responsive synaptic state. In contrast, during the night spontaneous glutamate release is low resulting in decreased basal action potential firing. However, decreased postsynaptic membrane conductance facilitates a high fidelity of synaptic throughput and potentiated post-stimulation bursts. Thus, at night, the synapse

has low basal tone and is highly responsive to incoming vagal afferent signals. **C)** Schematic drawing proposing the relationship between each oscillating component within ST afferents and NTS neurons. The axon terminal represents vagal afferents from the solitary tract. Increased glutamate release and membrane conductance enhance firing at rest during the day; while, reduced glutamate release during the night combined with increased membrane resistance enhances afferent evoked AP firing. The symbol ‘g’ represents a change in conductance/membrane resistance.

825 FIGURES

826

827 **FIGURE 1:**

828

829

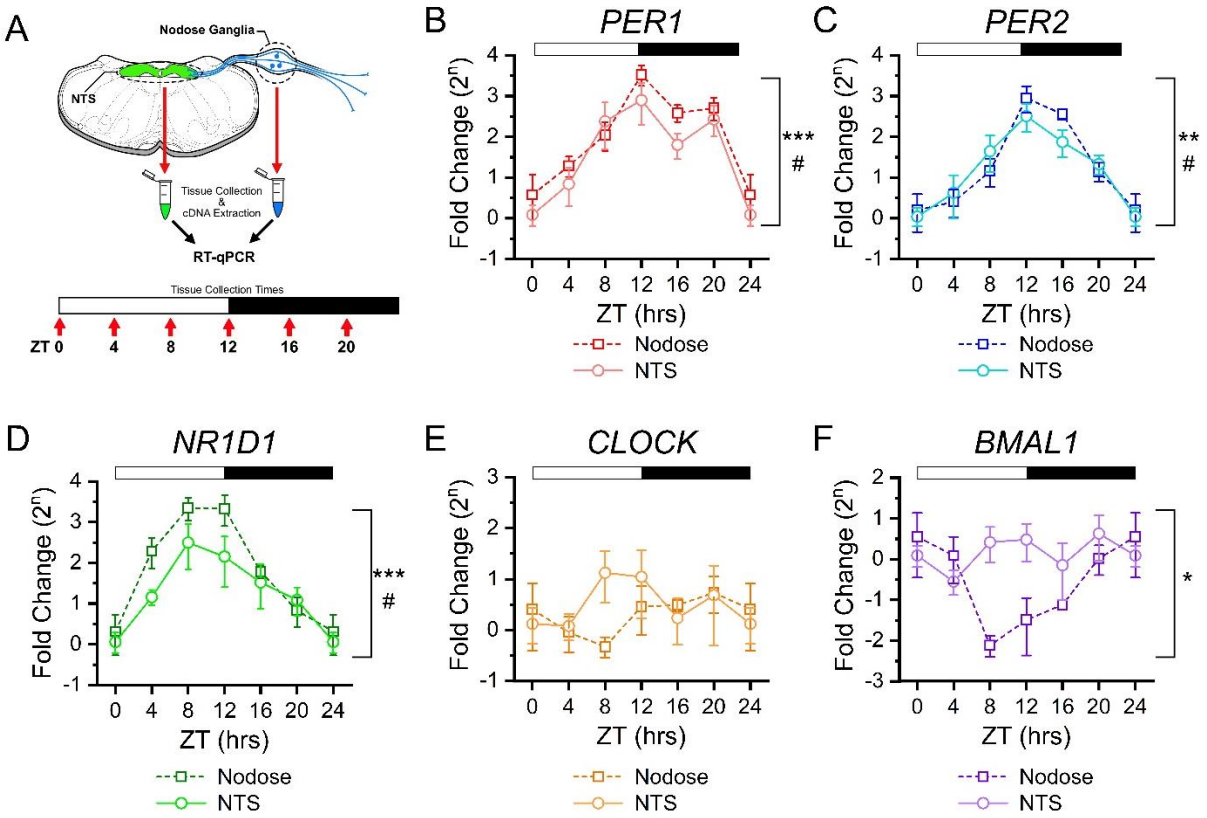

830

FIGURE 2:

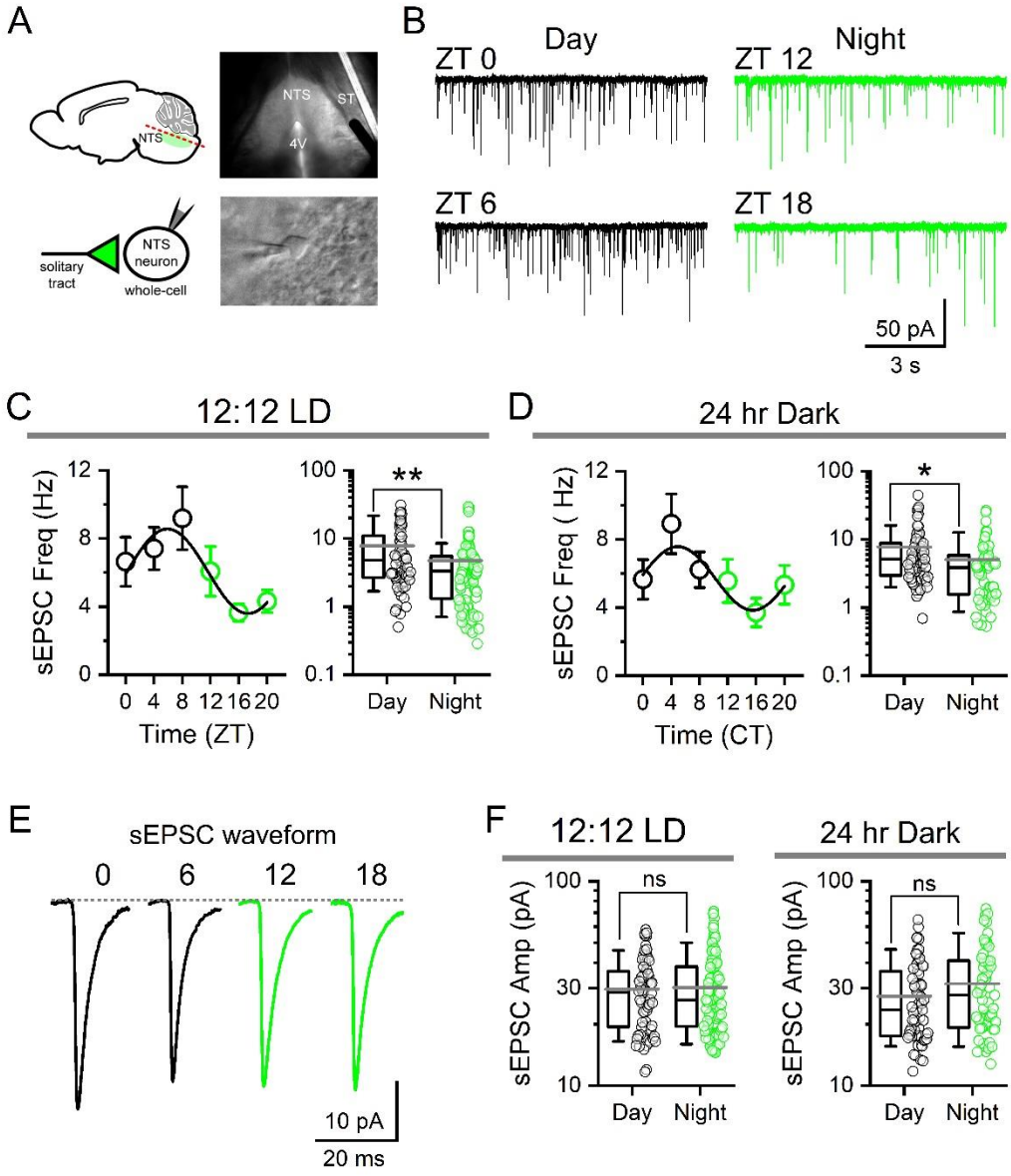

833 **FIGURE 3:**

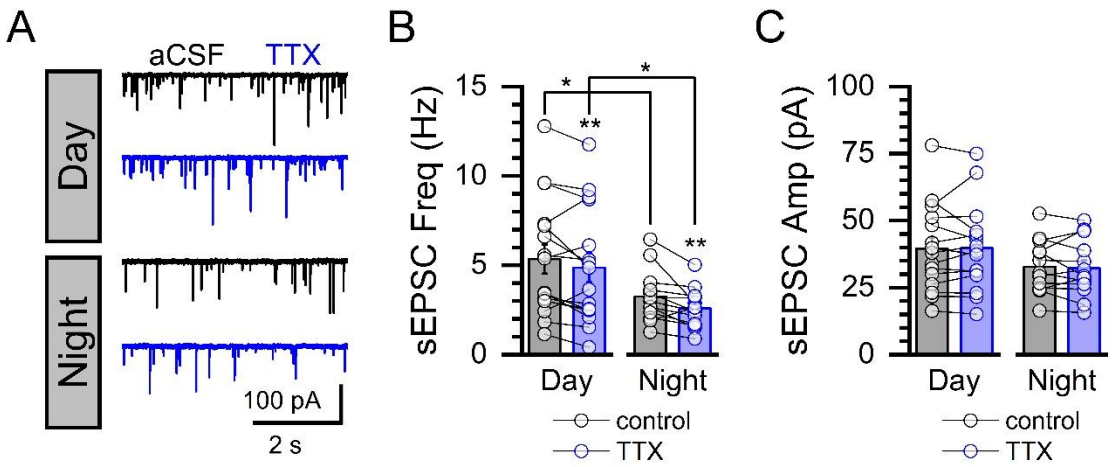

834

835 **FIGURE 4:**

836

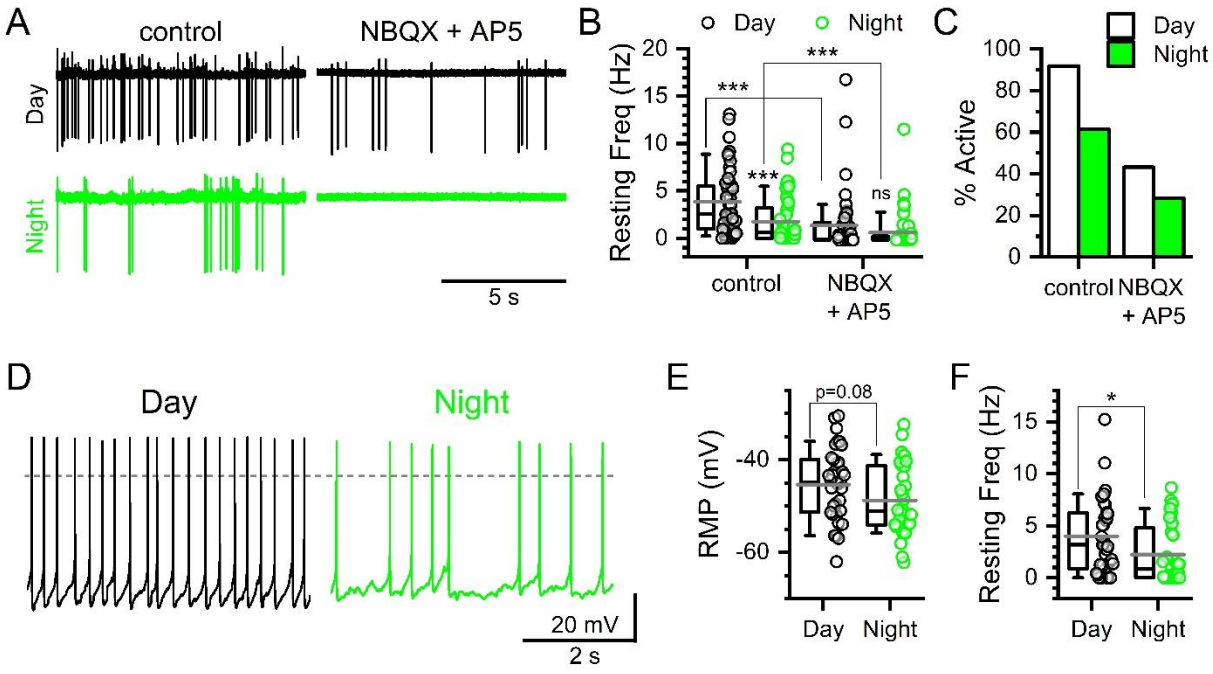

837

838 **FIGURE 5:**

839

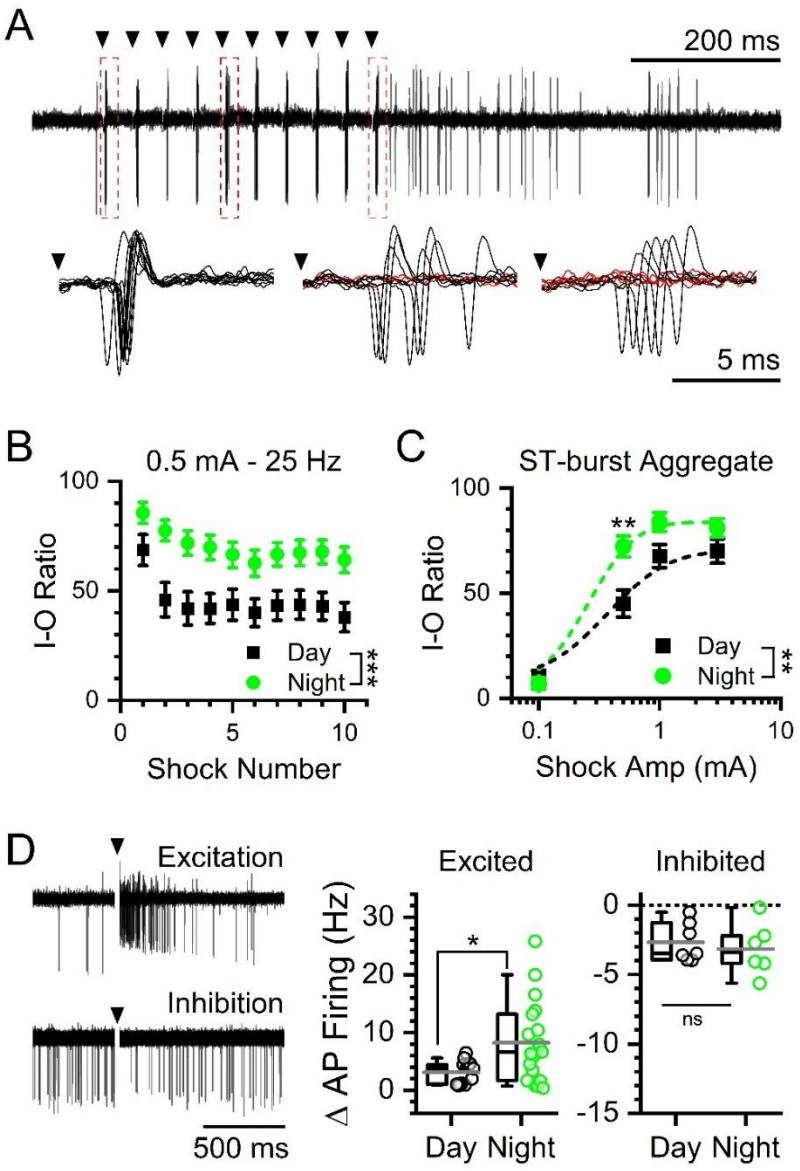

843 **FIGURE 6:**

844

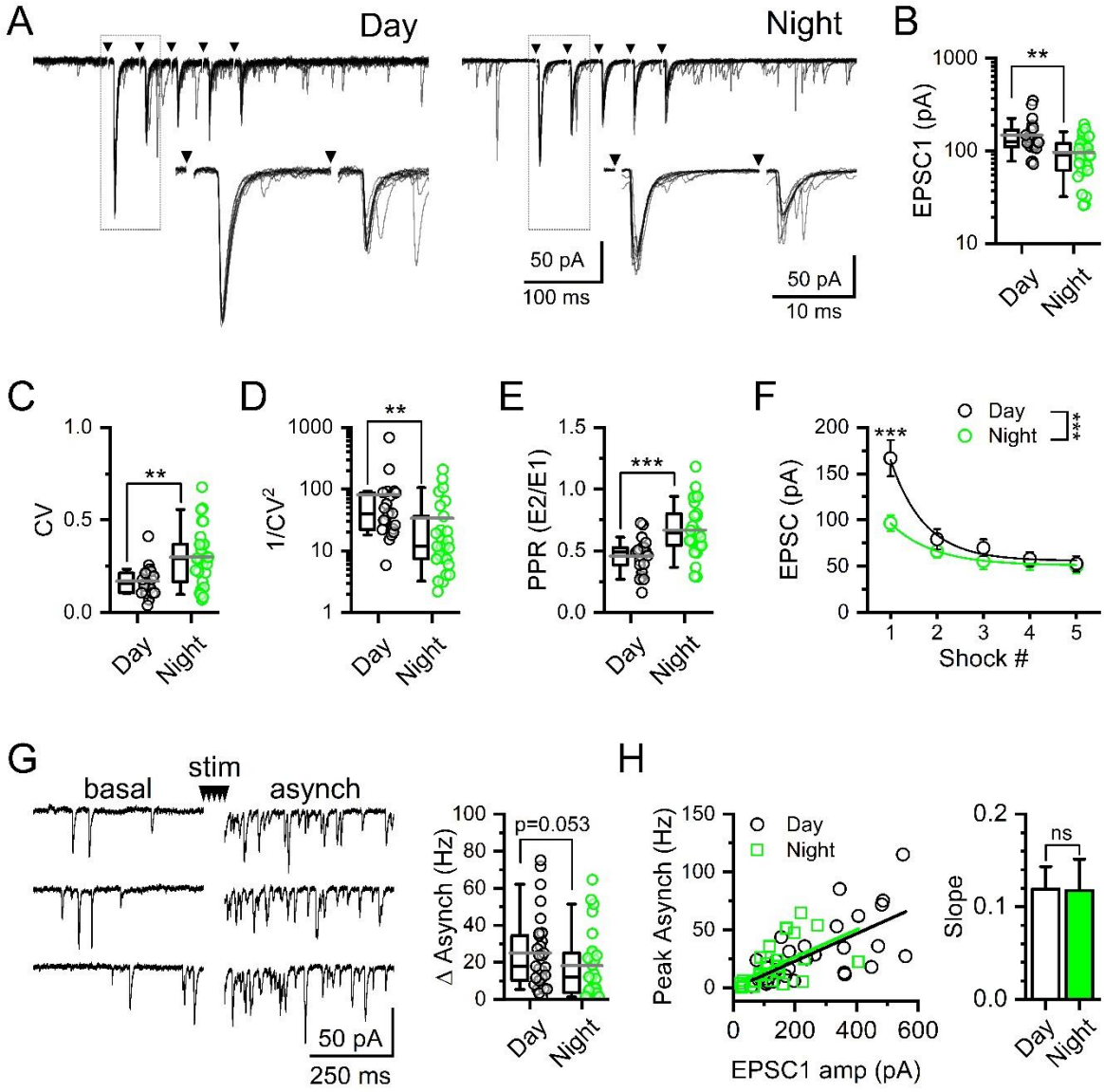

845

846 **FIGURE 7:**

847

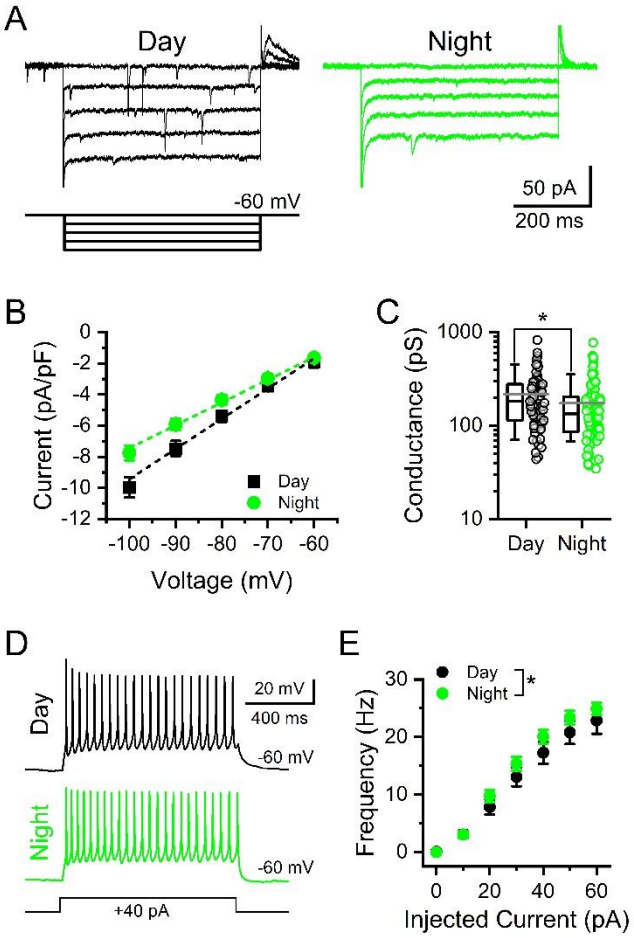

849 **FIGURE**

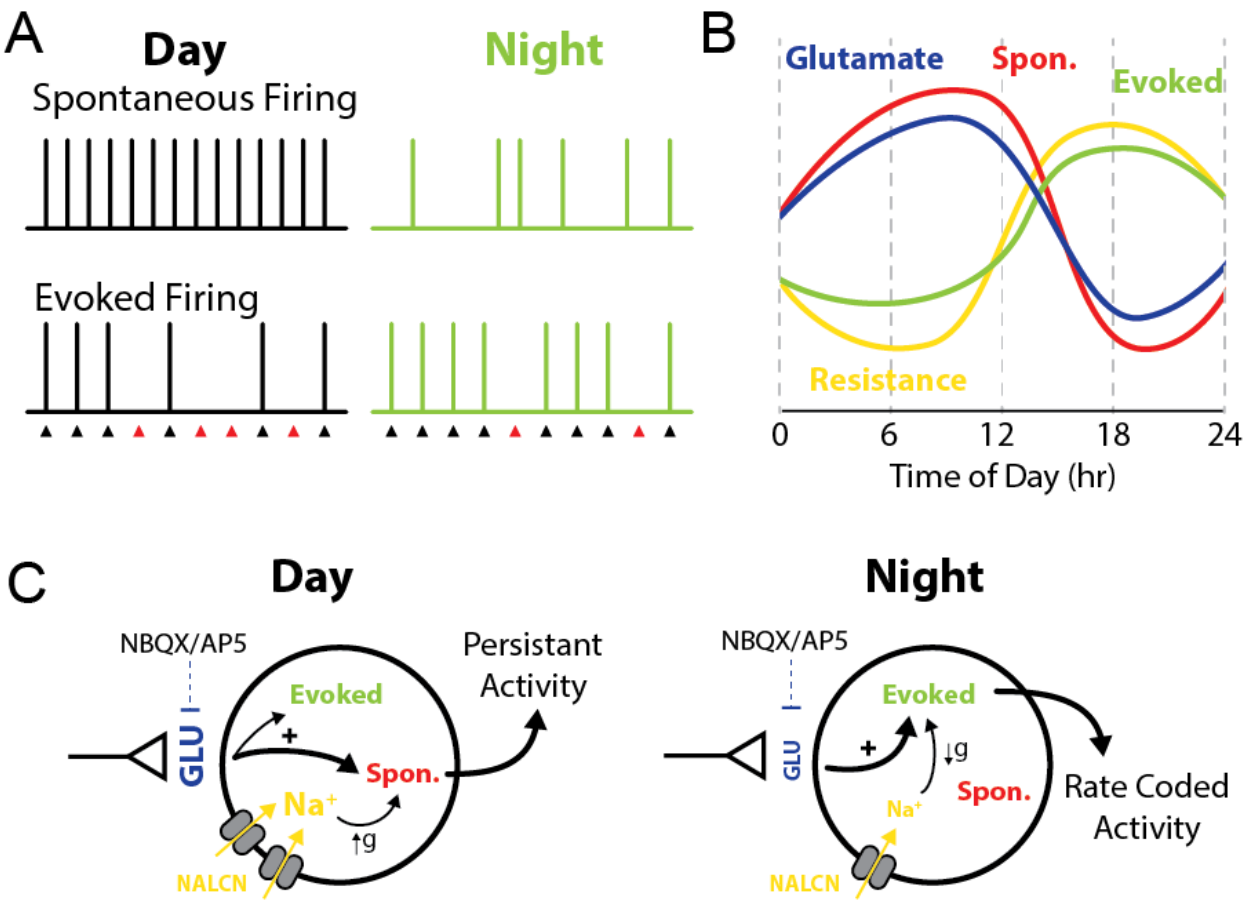

850